Fusion of Surface Ceilometer Data and Satellite Cloud Retrievals in 2D Mesh Interpolating Model with Clustering

Konstantin Khlopenkov [a], Douglas Spangenberg [a], William L. Smith Jr.[b]

[a] Science Systems and Applications, Inc. Hampton, VA, USA
[b] NASA Langley Research Center, Hampton, VA, USA

ABSTRACT

For accurate cloud ceiling information, a data fusion approach is proposed that utilizes satellite data to extend surface station information to much wider areas. Cloud base height (CBH) retrieved from satellite observations provides for much larger spatial coverage and higher resolution. The direct comparison of GOES-16 CBH with surface station ceiling yields a local bias that has to be corrected for in the initial GOES-16 cloud base information. This sparsely sampled bias correction presents an irregular 2D mesh of control points, which is then interpolated by constructing a continuous smooth field using polyharmonic splines. The influence of remote stations is restricted by grouping the control points into clusters depending on an effective distance. This cluster-based approach allows for constructing separate spline surfaces corresponding to physically different clouds. The obtained continuous bias correction function is then applied to the entire GOES-16 pixel level CBH except for areas far away from surface stations in data sparse regions such as offshore. The described method is currently being tested using daytime-only observations over the central and eastern United States. Overall, this approach has potential to provide more accurate, high spatial resolution cloud ceiling information for the aviation community.

Keywords: Remote sensing, cloud base height, cloud ceiling, clustering, image processing, interpolation, thin plate spline.

1. INTRODUCTION

Flight planners and pilots require accurate cloud ceiling information to conduct safe and efficient operations. Low visibility due to the presence of low cloud ceilings at airports can disrupt departures and arrivals causing delays and cancellations, leading to financial loss to private and commercial aviation. This disruption happens most often for commercial airlines when cloud ceilings are reported to be under 1,000 ft. Overhead sky conditions are reasonably well observed at many airports using a combination of human and ground-based sensor measurements, including ceilometers. Over smaller airports and in other areas where surface cloud ceiling observations are not available, cloud ceiling and visibility are not well known. This complicates aircraft operations, including small planes, helicopters and airborne medical and rescue flights. For those areas where surface cloud ceiling observations are missing or not available, a data fusion approach is proposed that utilizes satellite data to extend surface station information to much wider areas. Compared to surface observations, cloud base height (CBH) retrieved from satellite observations provides for a much larger coverage and higher spatial resolution. The direct comparison of GOES-16 CBH with surface station ceiling yields a local bias that has to be somehow corrected for in the GOES-16 cloud base information.

The data fusion algorithm described in this paper facilitates such a correction to the satellite retrieved CBH by means of a spatial interpolation of the sparse station observation. This method is currently being developed and tested using daytime-only observations over the central and eastern United States. Two independent sets of cloud-covered surface stations are randomly selected so that one can serve to develop the method with the other being used for validation. The overall goal is to utilize direct observations of cloud ceiling from the surface station network to better constrain satellite sensitivity to cloud height, cloud layering and thickness, thereby improving satellite cloud base retrievals at high spatial and temporal resolution.

2. DESCRIPTION OF INPUT DATA

The inputs needed to develop the hybrid surface station-satellite product include cloud ceiling measured by Automated Surface Observing System (ASOS) and Automated Weather Observation System (AWOS) ceilometer stations. Half of the full set of available cloudy station locations was randomly selected to develop the interpolation method described below, leaving the remaining set for validation purposes. The GOES-16 cloud property retrievals[1] used in this study include cloud optical depth, cloud phase, cloud effective temperature, and CBH. Empirical relationships involving cloud optical depth and cloud temperature are used to calculate cloud thickness. The GOES-16 cloud top height and thickness are then used to obtain CBH. To better separate clouds having different ceilings, five cloud types are defined to include water, supercooled water, optically thin ice, optically thick ice, and optically thick ice over low layer clouds. An optical depth of 10 is used to separate the thin and thick ice types. Inspection of GEOS-5 or MERRA-2 model maximum relative humidity (RH) in low layers is used to determine likely presence of low-mid clouds below thick ice using a 93% RH threshold. Although multilayer, or overlapping, cloud structures are quite frequent, the satellite cloud retrievals used in this study are taken to be composed of a single layer with the integrated effects of all clouds layers combined into one for multi-layered systems.

For each synoptic hour, surface observations are matched with satellite cloud product retrievals from GOES-16 using the images at 45 and 00 minute past the hour. For the matching process, the maximum allowed time difference between the surface observation and satellite is 7.5-min although it would have to increase for operational purposes given that surface observation times are clustered at the end of each hour with satellite times spread evenly across the hour. GOES-16 pixels falling within 20-km radius from the surface stations are averaged and the dominant cloud type is then selected for comparison with the station ceiling. The satellite CBH and station ceiling are both represented in terms of altitude above sea level.

Figure 1 presents a map of ceilometer station locations grouped by their corresponding dominant cloud types identified from GOES-16 retrievals. Stations of different cloud types are assigned to different groups or clusters and then a two-dimensional (2D) spline interpolation is constructed for each of the cluster independently. This helps the overall smoothness of each interpolating fields by removing the steep transitions between clouds at different height levels and

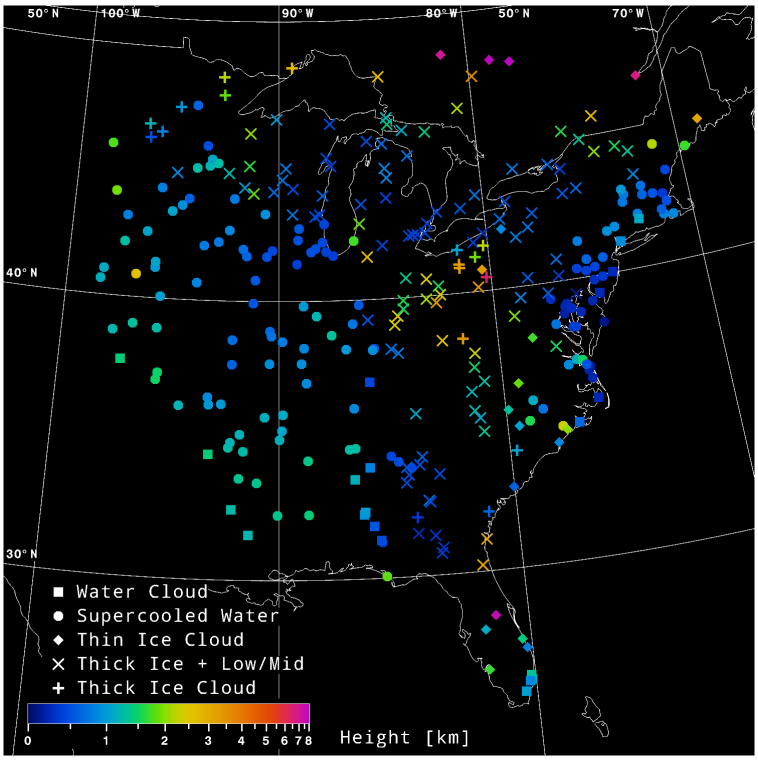

Figure 1. Locations of ceilometer stations selected from the 17 UTC hour on 15 Apr 2018 with their measured cloud ceiling shown in color. Different symbols show the 5 cloud type retrieved from GOES-16.

even enables a multi-layer interpolation by allowing the interpolated fields of different cloud types to overlap over the same area.

3. INTERPOLATION METHOD

The problem of predicting cloud ceiling in remote areas based on the measurement from ceilometer stations can be classified as constructing an interpolating two-dimensional field $f(x,y)$ on irregular (i.e. non-Cartesian) mesh of points. The geographic locations of the observing stations form a set of x_i, and y_i coordinates of the mesh vertices (called control points) and the station observed ceiling SOC_i are used as the values of the function f_i that have to be interpolated. An efficient and stable interpolation can be realized by using polyharmonic splines. In two dimensions, this can be implemented by constructing a thin plate spline (TPS)[2]:

$$f(x,y) = \sum_i w_i \varphi(r_i) + v_0 + v_1 x + v_2 y \tag{1}$$

where is r_i is the Euclidian distance from the current location (x,y) to each of the control points:

$$r_i = \sqrt{(x-x_i)^2 + (y-y_i)^2} \tag{2}$$

and $\varphi(r)$ is the radial basis function:

$$\varphi(r) = r^2 \ln r \quad \text{if } r>0, \text{ and } \varphi(0)=0 \tag{3}$$

The parameters w and v have a closed-form solution and can be easily computed by solving a linear system of equation[2]. The main advantage of the polyharmonic spline interpolation is that very good interpolation results are usually obtained for scattered data without performing any "tuning", so automatic interpolation is feasible.

In order to achieve the isotropy of distances between any two geographic locations, all the input data including satellite images and the surface station locations have to be remapped into a conformal geographic projection. The straight-forward pixel distances in that projection can then be used as the Euclidian distances in Equation (2) with high enough accuracy. For this study, we have chosen the Lambert conic conformal projection with one standard parallel of 40°N, the reference longitude of 90°W, and the nominal pixel resolution of 2 km/pixel. An input image is then reprojected by means of a so-called inverse remapping, when for every pixel in the output grid, its latitude and longitude are sought in the input geolocation arrays provided with the satellite image. This is implemented by means of the concurrent gradient search[3]. This search yields a fractional position in terms of the input image coordinates, which is then used to interpolate the adjacent input values by means of a 6×6 Lanczos resampling function. The interpolated sample is finally stored at the current location in the output grid. This inverse mapping process has two main advantages: (a) it ensures that all output pixels are filled with valid data, and (b) the interpolation is performed in the input pixel/line space where samples are aligned in a regular grid, which allows for straightforward resampling even with higher order polynomials.

An example of TPS interpolation over a set of 137 surface observations is shown in Figure 2a. This is the same case of 17 UTC 15 Apr 2018 with only stations where the cloud type was identified as “Supercooled Water Cloud”. It can be seen that the interpolating function $f(x,y)$ goes through all the station data (by the definition) and is also reasonably stable and smooth in areas with a good coverage by surface stations. Away from the stations, the obtained 2D field becomes an extrapolation that is guided mostly by the gradient based on the nearby station data. This causes overshooting of the interpolated field with the $f(x,y)$ going well over the highest observed station value (orange colored areas in Figure 2) as well as to extreme lows of zero level and below (enclosed areas shown as black).

The main question remaining here is how to make the interpolated cloud ceiling change gradually from the observing station data in their vicinities to the satellite retrieved CBH far away from the stations where only satellite observations are available. To answer this question, we need to analyze the behavior of the obtained interpolated field at the infinity. The TPS formula in Equation (1) contains a constant term v_0 followed by the two linear terms, which all describe a 2D plane that would be obtained by the least square fitting of the linear solution to the station values f_i . This design of the polyharmonic spline allows separation of the non-linear part of the solution (i.e. the curvature of the interpolated field) from the linear component (i.e. vertical offset and the overall slope). A simplified form without the linear terms

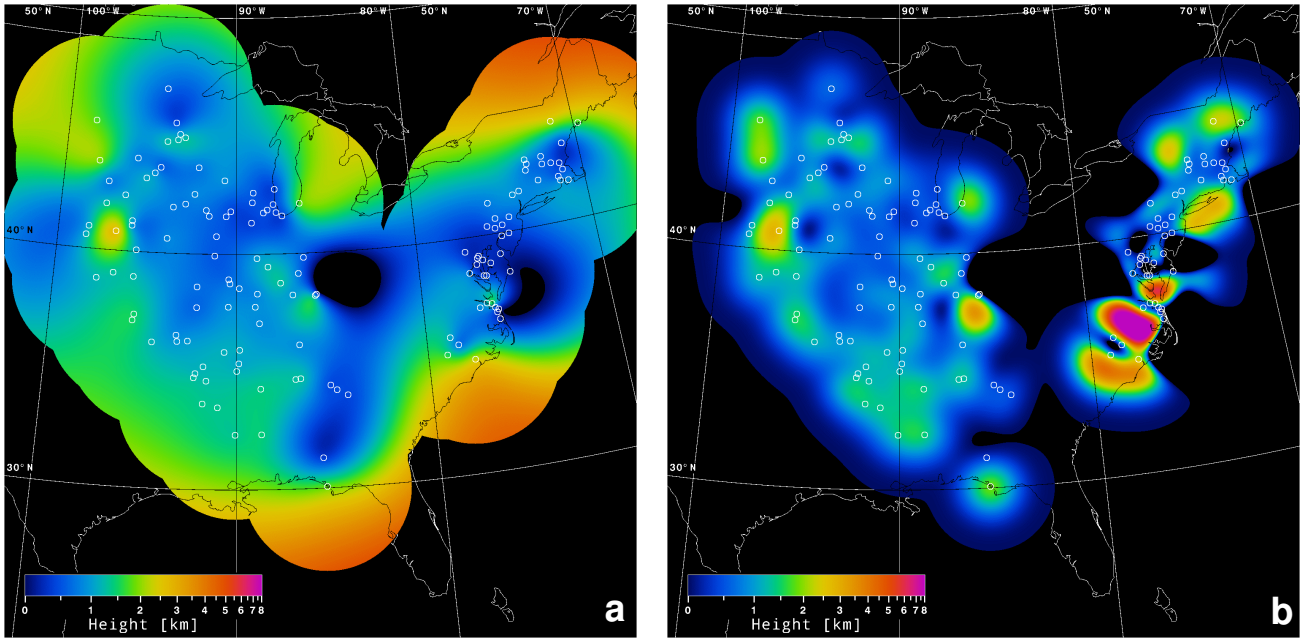

Figure 2. a) Interpolation of ceiling observation data (white circles) by means of the 2D thin plate spline. Interpolation is limited to the maximum distance of 400 km from the nearest station. Only stations with the cloud type identified as "Supercooled Water Cloud" are used here. The stations were selected from the 17 UTC hour on 15 Apr 2018. b) Interpolation of the same set of station data using Gaussian as the radial basis function with the characteristic distance σ of 50 km.

$$f(x,y) = \sum_i w_i \, \varphi(r_i) \tag{4}$$

yields a solution that has a zero offset and no slope by trading off some smoothness of the obtained field. In reality, this does not solve the problem of overshooting at the infinity because the extrapolated field is, in fact, non-linear (see the orange colored areas in Figure 2) and that cannot be compensated by removing the linear trend.

Another possible alternative to the radial basis function (3) is the well-known Gaussian function, which, on the contrary, tends to zero at infinity with a characteristic distance σ, which also allows for some tuning. An example of interpolation over the same dataset with the radial basis function (3) replaced with the Gaussian function is shown in Figure 2b. As expected, the interpolated field drops to zero level far way from the stations and the rate of this decrease can be controlled by adjusting σ. We used the characteristic distance σ of 50 km in this example to approximately describe the range of reliable measurement by the station ceilometer.

The essential idea allowing us to fuse the interpolated ceiling with the satellite retrieved CBH is to interpolate not the original ceiling data SOC_i but rather its difference from the CBH:

$$f_i = \Delta H_i = CBH_i - SOC_i \tag{5}$$

The interpolated result $f(x,y)$ is then subtracted from the CBH at every pixel to obtain the fused height F:

$$F(x,y) = CBH(x,y) - f(x,y) \tag{6}$$

At station locations, $F(x_i, y_i)$ yields the original ceiling data meaning that the fused product relies on ceilometer measurements near the observing stations, whereas away from the stations where $f(x,y)\rightarrow 0$, the result falls back to satellite retrieved CBH as no ground based correction is available.

This idea works as described with the Gaussian based interpolation; however, the problem is that the interpolated field in Figure 2a is not as smooth as the TPS based one shown in Figure 2b. The Gaussian based interpolation has many overshoots and saturated regions even in the areas between stations. Increasing the characteristic distance σ helps flattening to some degree the inner areas where stations are dense but leads to even stronger overshoots in areas where stations are sparse. On the other hand, the TPS using the radial basis function (3) is much more smooth and stable overall with the only drawback of not decreasing to zero far away from all stations, which effectively prevents the height difference approach based on Equations (5, 6).

To overcome this problem, we introduce a spatial correction designed to make the interpolated field decrease gradually to zero with growing distance from the nearest station:

$$f_c(x, y) = (1 - d^2)^2 \, f(x, y) \tag{7}$$

Here, $d = r/L$ is a normalized distance and L is some characteristic length describing the scale of the spatial decrease and this correction is calculated where $d<1.0$ or replaced with zero otherwise. For a typical L of 400 km, the correction factor is close to 1.0 in the areas of dense distribution of stations thanks to the quadratic functions in the Equation (7), and it gradually decreases to zero in the peripheral regions.

A comparison between the original TPS interpolation of the height difference (5) and the one with the spatial correction is shown in Figure 3. Similar the original height interpolation, the interpolated height difference presents a smooth field within the areas where stations are dense, which is shown as neutral light gray color in the Figure. In the peripheral regions, the interpolated field deviates significantly from zero and tends to saturate at extreme low and high values (see the left panel in the Figure). Once the spatial correction is applied, the saturated regions become a lot more stable and smooth while the whole field falls gradually to zero far away from all stations (see the right panel in the Figure).

It should be noted however, that the interpolated field now develops some artifacts like the uneven transitions between some boundary stations. See, for example, the horizontal orange line crossing the purple colored area at 33°N 86°W and the large orange colored area divided by yellow stripes around 43°N 77°W. Similar dividing stripes are noticeable in the

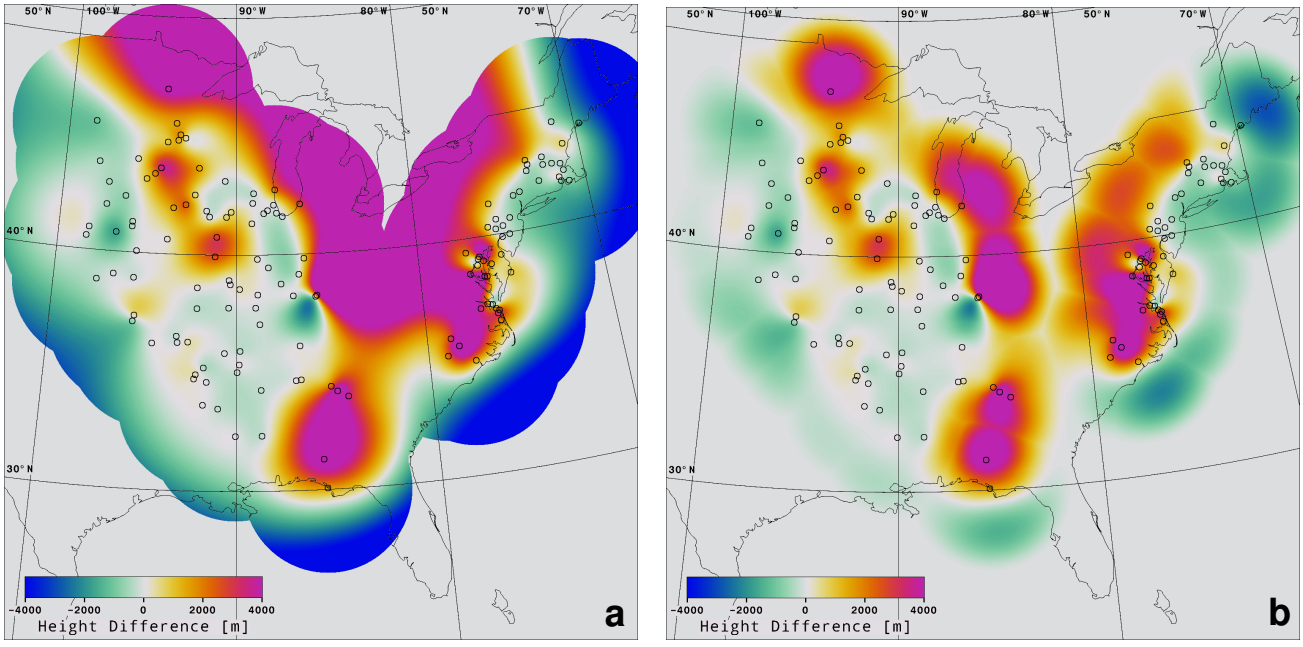

Figure 3. Interpolation of the height difference by using the TPS radial basis function (a) and the same interpolation with the spatial correction applied (b), which is based on the distance to the nearest station.

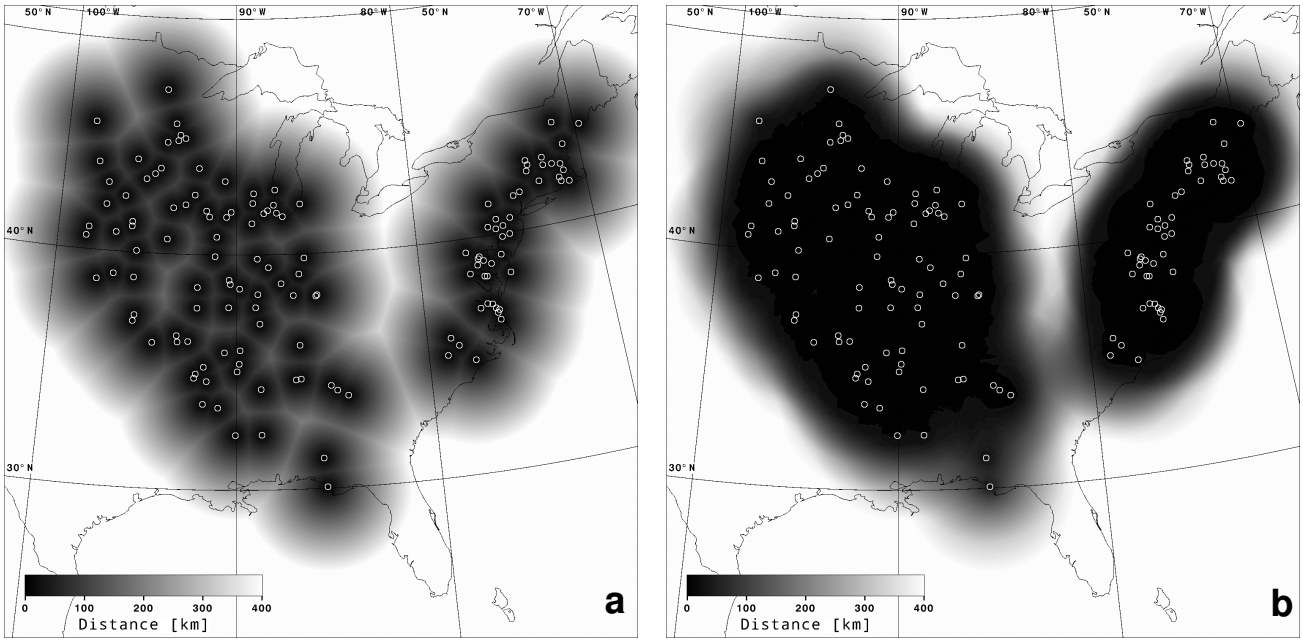

Figure 4. Comparison of distance maps obtained with two methods: distance to the nearest station (a); multiplicative aggregated distance (b).

green colored area along the Atlantic coast. All these artifacts are caused by the minimum distance r used in the Equation (7) which is based on the non-smooth $min(r_1, r_2)$ function. This function changes abruptly when the distances r_1 and r_2 to the two nearby stations become equal and this suddenly switches the effect on the correction function from one station to the other. This effect is more noticeable in Figure 4 a), where the distances to the nearest station are shown in the shades of gray.

In order to solve this problem, we introduce the following aggregated distance:

$$d_a = \sqrt{d_1 \cdot d_2 \cdot \ldots \cdot d_N}\,, \qquad 0 < d_i < 1 \tag{8}$$

This aggregated distance d_a presents a smooth function (shown in Figure 4 b) with the effect from all nearby stations combined in one formula similar to geometric average. Remote stations with $r>L$ are not included here. One can see that unlike the minimum distance field, the aggregated distance presents an evenly smooth field and the shape of the boundary of the dark area in the Figure 4b describes reasonably well the area covered by all ceilometer stations. The resulting interpolation with the spatial correction based on the aggregated distance d_a is shown in Figure 5a. The interpolated field is now free of the artifacts that were seen in Figure 3b. The saturation of the peripheral overshooting may appear stronger than in the case with the plain nearest distance but this can be easily adjusted by reducing the characteristic length L used for the distance normalization.

The main reason for the observed overshooting in some areas is actually in the high gradient of the interpolated field, which occurs when any two close stations have a too high difference in their vertical levels. Because those levels are, in fact, the height difference between the satellite retrieved CBH and the station observed ceiling SOC, we can assume that the high inter-station difference is caused by some uncertainty ε contained in the input CBH data:

$$f_i + \varepsilon = (\mathrm{CBH}_i + \varepsilon) - \mathrm{SOC}_i \tag{9}$$

If the high gradient in the interpolated field is to be reduced by some kind of a spatial smoothing then the adjustment that needs to be applied to the input data f_i can be attributed to the inherent uncertainty in CBH retrievals.

To implement the spatial smoothing, we first define the spatial gradient G_{ij} between any two stations i and j as follows:

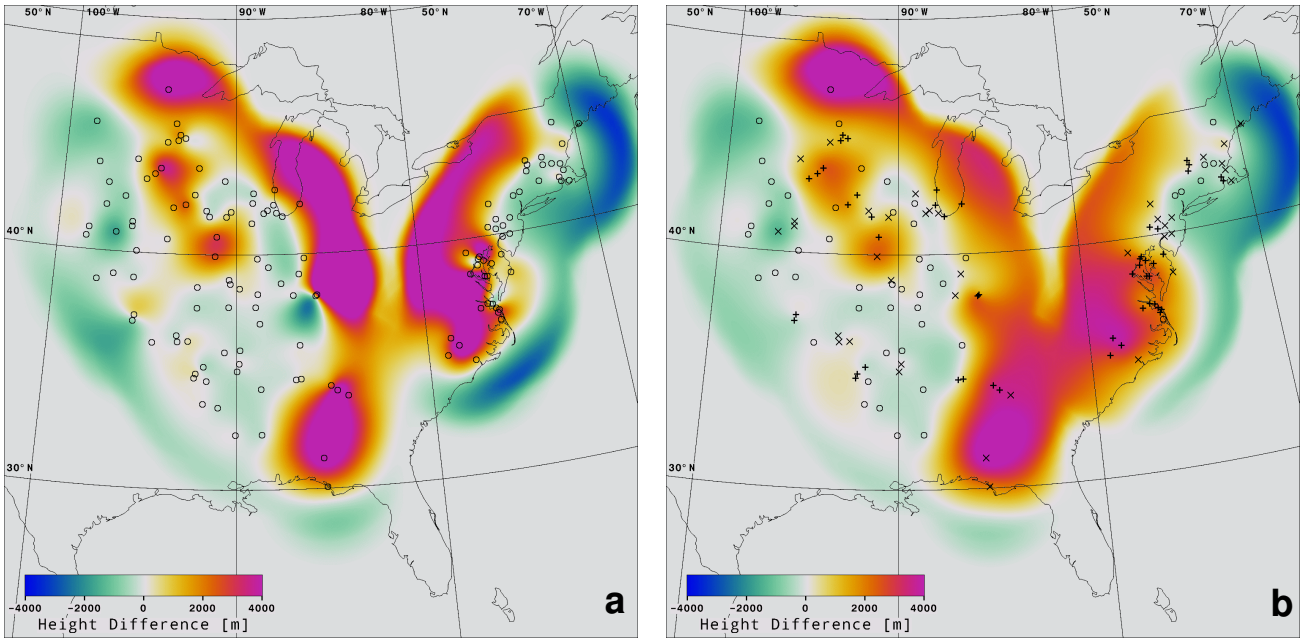

Figure 5. TPS interpolation of the height difference with the spatial correction applied, which is based on the aggregated distance d_a (a); same interpolation with the station data pre-processed by the dynamic smoothing (b).

$$G_{ij} = \frac{|f_i - f_j|}{r_{ij}^2} \tag{10}$$

where r_{ij} is the Euclidian distance between the two stations in pixels (the resolution is 2 km/pixel) and f is measured in meters. The squared r emphasizes the interaction between the closest stations making the smoothing process more localized. Then the adjustment to the station data f is implemented as follows:

$$f_i' = \bar{f} - \frac{\bar{f} - f_i}{1 + s\,G_{ij}} \tag{11}$$

where $\bar{f}$ is the average between the two stations, f_i is any station in the pair, and s is a smooth strength, typically 0.5. Thus this adjustment is dynamic in that it is stronger when the difference between the two stations is higher. This smoothing is run over all pairs of stations having $sG_{ij} > 0.2$ and is applied in the order of decreasing their mutual gradients G_{ij}. The ordering helps limiting the smoothing process to the most differing pairs of stations.

An example of the interpolated height difference pre-processed by the dynamic smoothing is shown in Figure 5b. Stations shown with circles have their original data, those with crosses have been adjusted with $sG_{ij} < 0.5$, and the plus signs indicate stations smoothed with $sG_{ij} \geq 0.5$. Comparing to the last result without smoothing (Figure 5a), one can easily notice that the interpolating field has become more even and stable overall. The remote stations between 80°W and 85°W are now connected with a more constant color without sharp breaks. The purple areas are overall significantly weaker and the blue band around South East coast is reduced as well.

In some cases, even when the stations belong to the same cloud type, they may still form more than one distinct groups (as in the example analyzed here) or their vertical levels may be too different. In that case it may be worth separating them in different clusters and subsequently constructing two or more independent spline interpolations. To quantify the separation between any two points we need to introduce a concept of effective distance D_{eff} between any two nearby stations. When D_{eff} exceeds a certain threshold, the stations are considered to have a too high separation and they are assigned to different clusters. The threshold is fixed at 1.0 and the effective distance is calculated as follows:

$$D_{eff} = w_r \cdot 0.006\, r_{ij} + w_c \frac{\left| f_i - f_j \right|}{0.006\, r_{ij} + 0.8} \tag{12}$$

where w_r , w_c are weights that are fine-tuned manually in order to achieve the best balance between the influence of the geographic distance and the difference between the ceilings observed by the two stations. Thus, if two stations are too far from each other or their vertical levels are too different then they will be assigned to different clusters, which may help to emulate the naturally occurring boundaries between different clouds. On the other hand, we found that the interpolating surface is generally more stable if more control points are added to the cluster. From our preliminary tests, the weights $w_r = 0.2$ and $w_c = 0.3$ appear to work very well.

4. DISCUSSION AND CONCLUSION

Once the optimal interpolation is obtained for each cluster, the results can be combined into a single height difference field. This is implemented by taking the cloud type for each satellite pixel and selecting the interpolation from the corresponding cluster. If more than one cluster exists for that cloud type then the ownership is resolved by means of the effective distance from Equation (12). The resulting field is shown Figure 6, where clusters of different cloud types are shown with different color hues. This meteorological case has a strong mid-latitude low pressure system and associated cold front moving through the eastern half of the United States. Deep ice-topped clouds are shown as yellow shades in Figure 6. Most areas are light yellow, indicating the SOC was significantly lower than satellite CBH. In deep clouds, the higher optical depth frequently causes satellite CBH to be too high, as it cannot detect with certainty the presence of low-level clouds under the optically thick ice cloud. Thin ice cloud base heights were also overestimated by the satellite over central FL and along the SC coastline likely because thin boundary layer clouds could not be detected. Conversely, the dark green areas in southern Canada indicate the satellite CBH was underestimated. This occurred in the presence of relatively thin ice cloud over a snow surface where the actual scene detected by the satellite was from a significant depth

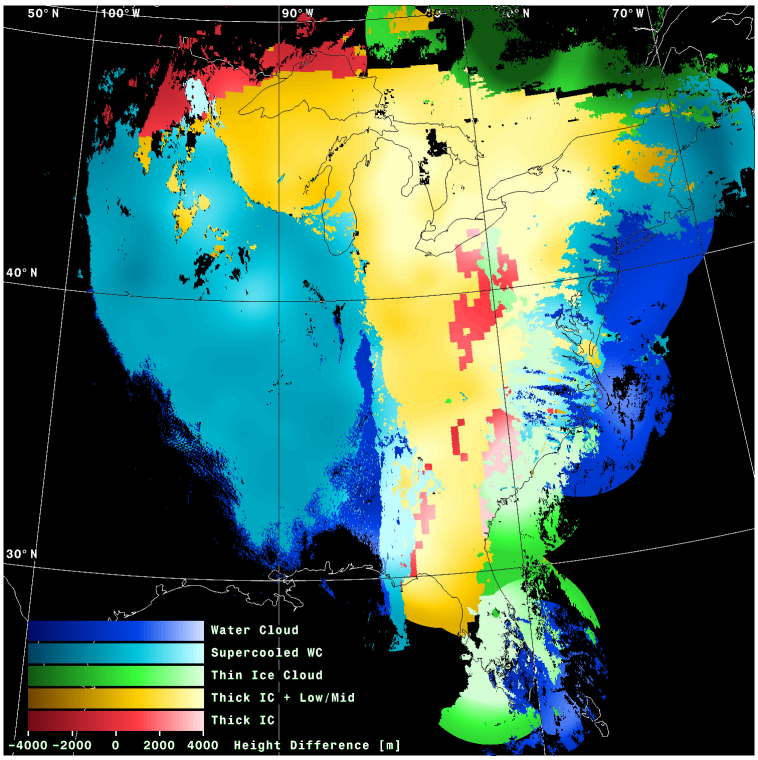

Figure 6. Interpolated height difference composed of several clusters corresponding to different cloud types. The GOES-16 image data is valid at 16:45 UTC 15 Apr 2018.

below actual cloud top. The possibility exists that it wasn't fully compensated for in the cloud height retrievals, causing the cloud to be placed too low. Another source of error in the satellite CBH is that temperature inversions caused the cloud to be placed too low in the thermal profile. Well behind the cold front, the large area of cyan in Figure 6 representing supercooled water cloud shows the satellite CBH and SOC are in relatively good agreement with some discrepancy over far western IL and eastern NE probably due to the low-level temperature sounding structure used to derive satellite cloud altitude. There were also areas along the AL-GA border where supercooled water cloud base height was significantly overestimated by the satellite likely due to large changes in thermal profiles near the cold front with the satellite recognizing it as mid-level cloud.

The actual GOES-16 CBH valid at 16:45 UTC 15 Apr 2018 and corresponding fused height (obtained from Equation 6) for the 17 UTC hour observation are shown in Figure 7a and b, respectively. The values along and ahead of the cold front appear much more realistic in the hybrid product with lower cloud bases observed throughout much of the image. A small area of higher cloud ceilings around 4-km MSL in Figure 7b appears from eastern OH to eastern KY corresponding to an area where model low-level RH wasn't high enough to indicate the presence of low-mid clouds below thick ice (red color in Figure 6). This is in agreement with higher station ceilings reported across that area. In both Figure 7a and b, the cloud ceiling is 0.5-2 km MSL behind the cold front with a noticeable lowering of ceilings in the hybrid product from western IL to northern IA near center of the mid-upper level low pressure system. A more complicated pattern is seen over FL with all 5 cloud types observed over the state. More stations applied operationally or slight modification of the current approach might help to sort out the pattern of multiple cloud types over small areas. Also, slight changes in the cloud type definitions might yield better results, for example, using any ice clouds with water or supercooled water clouds below instead of just thick ice with water or supercooled water clouds below.

The sparsely sampled bias correction presented an irregular 2D mesh of control points, which can be interpolated by constructing a continuous smooth field using polyharmonic splines. The influence of remote stations is restricted by grouping the control points into clusters depending on an effective distance, which accounts for geographical distance, the observed ceiling difference, and the satellite identified cloud type. This cluster-based approach allows for constructing separate interpolating fields corresponding to physically different clouds. The obtained continuous bias correction function is then applied to the entire GOES-16 pixel-level CBH except for areas far away from surface stations in data sparse regions such as offshore. In the areas without surface stations, a mean bias correction can be applied that would be taken from all stations of a given cloud type for each satellite image. The described method is currently being tested using daytime-only observations over the central and eastern United States. Two independent sets

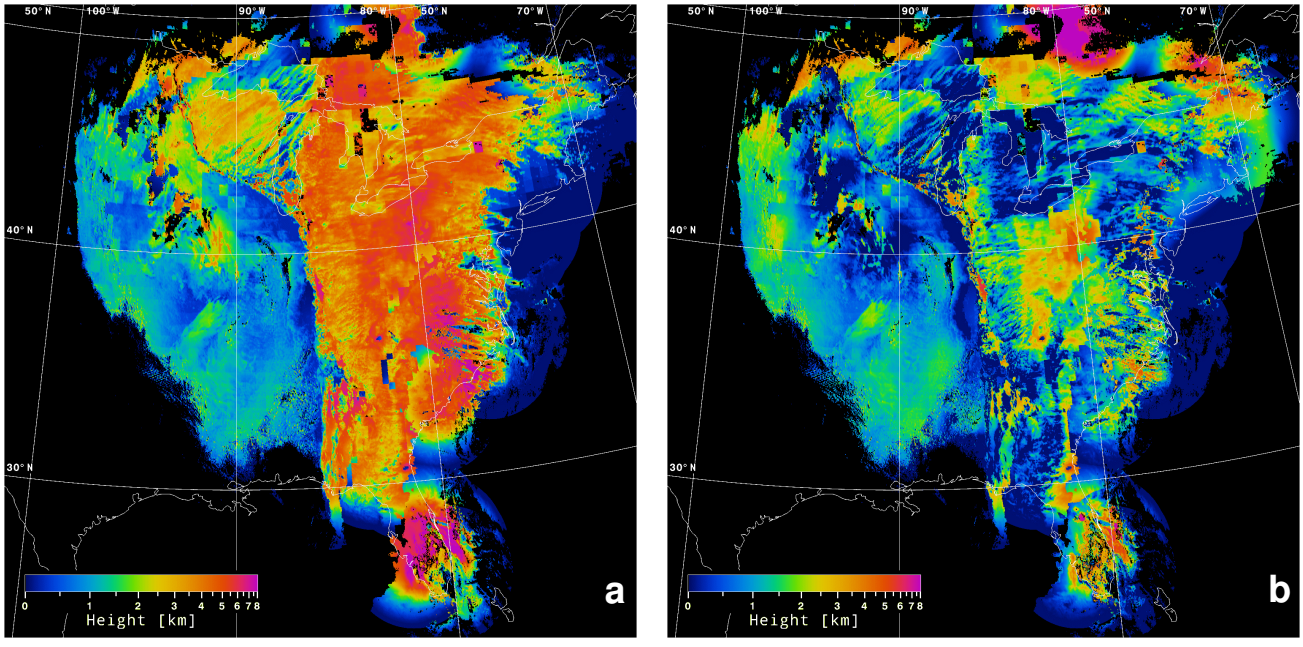

Figure 7. Comparison of the cloud base height products: the original satellite retrieved cloud base height (a); cloud base height fused with ceilometer observations interpolated with the modified TPS algorithm. The 16:45 UTC 15 Apr 2018 GOES-16 CBH was paired with the synoptic hour 17 UTC SOC.

of cloud-covered surface stations were randomly selected with one serving as control points and the other being used for validation. It was found that the RMS errors were significantly lower in this hybrid interpolation method compared to the satellite-only algorithm, and also the latter overestimated the cloud ceiling by 1.7-km in optically-thick ice-topped cloud systems, while the cluster-based interpolation yielded a near 0 bias. Overall, this approach exploits the synergy between advanced GOES-16 imager data, ground-based observations and model data over the U.S., and has potential to provide more accurate, high spatial resolution cloud ceiling analyses for the aviation community.

5. REFERENCES

[1] Minnis, P., S. Sun-Mack, D.F. Young, P.W. Heck, D.P. Garber, Y. Chen, D.A. Spangenberg, R.F. Arduini, Q.Z. Trepte, W.L. Smith, Jr., J.K. Ayers, S.C. Gibson, W.F. Miller, V. Chakrapani, Y. Takano, K.N. Liou, and Y. Xie., 2011: CERES Edition–2 cloud property retrievals using TRMM VIRS and Terra and Aqua MODIS data, Part I: Algorithms. IEEE Trans. Geosci. Remote Sens. 49, 4374-4400.

[2] J. Duchon, 1976, Splines minimizing rotation invariant semi-norms in Sobolev spaces. pp 85–100, In: Constructive Theory of Functions of Several Variables, Oberwolfach 1976, W. Schempp and K. Zeller, eds., Lecture Notes in Math., Vol. 571, Springer, Berlin, 1977

[3] Khlopenkov, K. V., Trishchenko, A. P., “Implementation and Evaluation of Concurrent Gradient Search Method for Reprojection of MODIS Level 1B Imagery,” IEEE Trans. Geosci. Remote Sens., 46(7), 2016–2027, doi: 10.1109/TGRS.2008.916633 (2008).